J. Phys. B: At. Mol. Phys. **20** (1987) 1121-1134. Printed in the UK

Electron impact single ionisation of multiply charged krypton ions

K Tinschert†, A Müller†, G Hofmann†, Ch Achenbach†§, R Becker‡ and E Salzborn†

† Institut für Kernphysik, Universität Giessen, D-6300 Giessen, West Germany
‡ Institut für Angewandte Physik, Universität Frankfurt, D-6000 Frankfurt, West Germany

Received 27 June 1986, in final form 1 August 1986

Abstract. Absolute cross sections $\sigma_{q,q+1}$ for electron impact single ionisation of Kr^{q+} ions ($q = 1, 2, 3$) have been measured for electron energies up to 700 eV by employing a dynamic crossed-beams technique. The experimental data significantly exceed the Lotz prediction for direct ionisation of Kr^{2+} and Kr^{3+} ions, indicating the importance of indirect processes for multiply charged Kr^{q+} ions. The observed ionisation thresholds of cross sections from the present measurements as well as of data from Danjo *et al* and Gregory *et al* indicate the presence of metastable ions in the parent ion beams. The influence of metastable states on the cross sections is discussed on the basis of Lotz calculations for direct ionisation from different excited states and differences observed in the experiments are rationalised.

1. Introduction

Electron impact ionisation of atoms and ions is one of the most important processes in astrophysical and laboratory plasmas. For the understanding and modelling of such plasmas, large amounts of cross section data are needed. Therefore, an increasing number of measurements on the ionisation of ions has been performed during the last few years and a considerable body of data has accumulated (see e.g. Tawara *et al* 1985). Theoretical description of electron-ion collisions and interpretation of the experimental data turned out to be difficult and, in general, theory is still unable consistently to predict the cross sections. More experimental data, especially on multiply charged ions, are needed, therefore, to test and guide theoretical calculations.

Experimental investigations and theoretical studies of triply charged transition-element ions (Falk *et al* 1981, 1983a) and measurements for singly charged alkaline-earth ions (Peart and Dolder 1975) exhibited significant contributions of excitation-autoionisation (EA) processes, which can even dominate over direct ionisation of an outer-shell electron. Experimental evidence exists for the general trend of increasing relative importance of EA along isoelectronic sequences (Crandall *et al* 1979, 1982, Howald *et al* 1986) and along isonuclear sequences with increasing initial ion charge state (Achenbach *et al* 1984, Griffin *et al* 1984). A further indirect ionisation mechanism was first predicted by LaGattuta and Hahn (1981) for the electron impact ionisation of Fe^{15+}: resonant recombination with inner-shell excitation followed by multiple autoionisation (RRMA). Griffin *et al* (1984) expected this process to contribute to the

§ Present address: Daimler-Benz AG, Stuttgart, West Germany.

0022-3700/87/051121+14$02.50

single ionisation of Xe^{6+} ions but so far no unambiguous experimental evidence for RRMA has been found. While direct single ionisation appears to be reasonably well understood, it is difficult to predict contributions from indirect ionisation processes such as EA and RRMA.

Extensive experimental studies were carried out on electron impact ionisation of the rare-gas ions Ar^{q+} ($q = 1, \ldots, 6$) by Woodruff *et al* (1978), Müller *et al* (1980, 1985a), Gregory *et al* (1983), Danjo *et al* (1984), Mueller *et al* (1985) and Howald *et al* (1986) and Xe^{q+} ($q = 1, \ldots, 6$) by Gregory *et al* (1983), Gregory and Crandall (1983), Achenbach *et al* (1984), Griffin *et al* (1984) and Danjo *et al* (1984). They revealed much information about the charge-state dependence of direct and indirect ionisation mechanisms. While in the case of Ar^{q+} ions, significant contributions of indirect ionisation processes could be identified only for $q = 5$ and $q = 6$, the measurements for the complex Xe^{q+} ions exhibited large enhancements in the cross sections for $q \geq 2$, which were attributed to EA processes especially from the 4d subshell.

Complementing our previous systematic investigations of electron impact ionisation of rare-gas ions, we present in this paper the results of cross section measurements for Kr^{q+} ions ($q = 1, 2, 3$). Contributions from different subshells and the influence of metastable ions in the parent ion beams are discussed.

2. Experimental technique

A detailed description of the experimental technique and the apparatus used for the present measurements was given in a previous paper (Müller *et al* 1985a). In short, beams of multiply charged krypton ions were continuously extracted from an electron-beam ion source (Müller and Salzborn 1979) and accelerated by a voltage of 10 kV. Ions of a certain charge and mass were separated by a 90° double-focusing magnet and collimated by a set of two apertures 36 mm apart from each other. Different sets of apertures could be moved into the ion beam line and so aperture combinations with diameters between 0.2 and 0.7 mm for each aperture could be chosen for cross section measurements. The ion beam of well defined diameter then entered the interaction region where it intersected at right angles with the intense ribbon-shaped electron beam which extended 60 mm in ion beam direction and reached a total current up to about 200 mA at 700 eV electron energy. The ionised product ions were separated from the parent ion beam by a second 90° analysing magnet and directed into a single-particle detector (Rinn *et al* 1982) while the parent ion beam was collected by a large Faraday cup. Complete transmission of the parent and the product ion beams was assured by test measurements involving iris apertures in front of the detectors and by the observation of flat-topped signal peaks (for details see Müller *et al* 1985a).

For a cross section measurement the electron gun was moved up and down across the ion beam. In the extreme positions the electron beam did not overlap with the ion beam, yielding an easy measurement of the background while both beams were 'on'. The count rate of the product ions was registered simultaneously with the digitised current of parent ions and the actual velocity of the electron gun movement, and was stored as a function of the electron beam position.

Figure 1 shows a typical spectrum of the raw data obtained by this procedure. The measured spectrum is divided into three sections. The first section (no I) contains the counts of the single-particle detector as a function of electron gun position. For

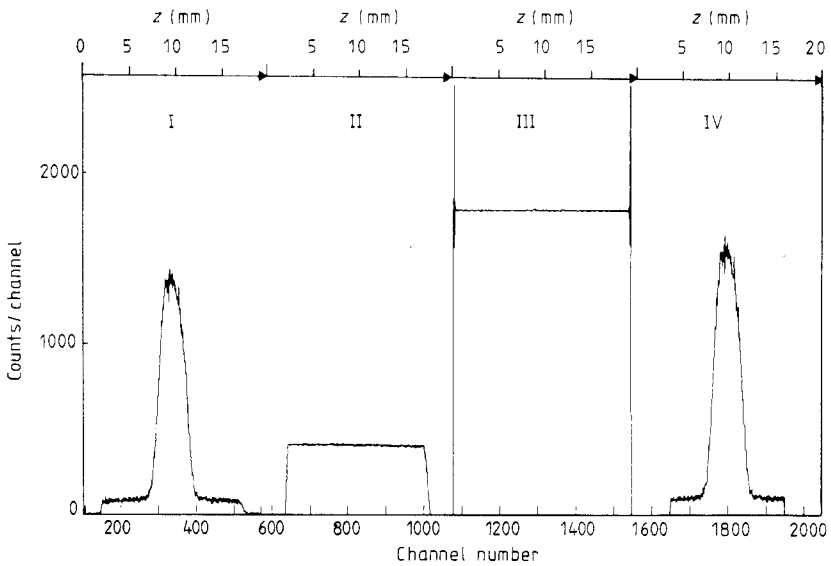

Figure 1. Typical MCA spectrum obtained for the process $e + Kr^{1+} \rightarrow Kr^{2+} + 2e$ at an electron energy of 150 eV showing (from left to right) the signals of the ionised ions (section no I), the accumulated parent ion charge (section no II) and the inverse velocity of the electron gun movement (section no III) as a function of electron gun position. Section IV of the spectrum is generated as described in the text by dividing the number of counts in one channel of section I by the number of counts in the corresponding channel of section II. For a convenient display the result is multiplied afterwards by a scaling factor.

each part of the spectrum, $z = 0$ designates the lowest and $z = 20$ mm the highest position of the electron gun. Only in the peak region do electron and ion beams overlap, and true electron impact ionisation events were registered on top of a constant background from stripping reactions which do not depend on the electron gun position. The second section (no II) of the spectrum displays the current of parent ions while the third section (no III) gives information about the velocity of the electron gun movement. For constant ion current and speed of gun displacement, the cross section is directly proportional to the total number of accumulated signal counts obtained during the overlap of electron and ion beams and inversely proportional to the total intensities of both beams no matter how these intensities are distributed across the sections of the beams. Thus it is not necessary to do a separate measurement of the form factor, which describes the beam overlap in a conventional crossed-beams experiment, and hence each ionisation cross section is determined independently and is absolute.

Different from the measurements of Müller *et al* (1985a) we have introduced an improvement in the data-taking procedure for product and parent ion rates as well as speed of gun movement. Pulses from the single-particle detector, the current digitiser and a fixed-frequency pulse generator are counted by three different scalers until the motor driving the electron gun has made a certain number of revolutions which corresponds to a displacement Δz of the electron beam. When the pre-fixed number of revolutions is reached, a computer reads and resets the scalers and the numbers of counts are stored in three corresponding channels of a multichannel analyser such that a spectrum as displayed in figure 1 is generated. The advantage of this technique is

the constant width Δz for each of the three corresponding channels in the spectra. Thus a formalism of cross section determination derived by Müller *et al* (1985b) can be employed which requires neither a constant speed of electron beam displacement nor a constant parent ion beam current.

For the determination of a cross section from raw data such as those displayed in the first three sections in figure 1, the number of counts in each channel of the signal section (no I) is divided by the number of counts in the corresponding channel of the section for accumulated ion charge (no II), which leads to the normalised data in the fourth section (no IV). The ionisation cross section σ can be obtained from

$$\sigma = \frac{S\Delta z}{MI_e\varepsilon} \tag{1}$$

where S is determined from the normalised data in section no IV. The factor S is the area of the peak (obtained with both beams overlapping) sitting on a constant background (obtained with complete separation of both beams). The factor M is given by

$$M = (v_e^2 + v_i^2)^{1/2}/(v_e v_i q e^2) \tag{2}$$

where v_e is the electron velocity, v_i the ion velocity, q the parent ion charge state and e the charge of an electron. Besides S and M only the total electron current I_e, the channel width Δz and the counting efficiency ε of the detector system used for the product ions enter equation (1).

In 'normal' cases such as the one displayed in figure 1 there is no difference in the cross sections resulting from the technique described above and the technique employed previously by Müller *et al* (1985a). For testing the new method we purposely modulated the ion beam current and the speed of the electron gun displacement during scans from $z = 0$ to $z = 20$ mm. Correspondingly the distributions in sections I, II and III of the raw data spectrum reflect these modulations. Especially the signal distribution—which is determined both by the actual (now z-dependent) parent ion current and the speed of the gun movement—is strongly influenced and may become indented; however, the smooth dependence is restored by the normalisation of the signal to the collected ion charge in corresponding channels, i.e. at given position z. The obtained cross section resulting from equation (1) is the same as before.

3. Uncertainties

The most important parameter for the evaluation of cross sections is the area S under the peak in the normalised spectrum (no IV in figure 1). Since it depends on the counting of random events it has a statistical uncertainty which we evaluated for a 95% confidence level. Because of the high ionisation efficiency of the electron beam and the possibility to sweep the electron beam up and down across the ion beam several times, a sufficient number of signal counts is accumulated so that the statistical error is typically less than 2%. Only in the threshold region where the signal-to-background ratio becomes much less than one do higher counting errors occur.

Systematic errors arise from the determination of the different experimental parameters that enter equation (1). The factor M including the electron and ion velocities has an uncertainty of ±1% due to errors in the measurement of v_e and v_i, which are estimated to be accurate within ±1%. The uncertainty of the measured total electron

current is within ±3%. The error in collected ion charge depends on the accuracy of the current-to-pulse-rate converter and is also within ±3%. The efficiency of the single-particle detector was determined to be $\varepsilon = 0.97 \pm 0.03$.

The probable total uncertainty is obtained as the quadrature sum of the statistical counting error at 95% confidence level and the individual systematic uncertainties estimated at a comparable confidence level.

The electron energy E_e is determined by the measurement of the voltage between cathode and interaction volume. Since we do not calibrate these measurements to a resonance or an excitation threshold, we have to allow an uncertainty of our energy due to the 0.5% uncertainty of the voltmeter, to contact potentials and eventually also to electron space-charge effects. Contact potentials are typically of order 1 eV. The maximum uncertainty ΔE_e of E_e due to the space-charge potential variation inside the electron beam was calculated by using a computer code which solves the Poisson equation in the presence of charged particles. ΔE_e amounts to $0.04 E_e$ and would result in a total energy width of less than 2 eV at the thresholds of the ionisation processes investigated in this paper. This has to be regarded as an upper limit for the error since we have strong evidence for large compensation of electron space charge by slow residual-gas ions (Müller *et al* 1987).

Previous ionisation experiments published by this group reproduced known ionisation thresholds in the range up to 100 eV to within ±1 eV, which is consistent with the above considerations.

Hence, we assume an uncertainty of $\max\{1\text{ eV}, 0.01 E_e\}$ for the electron energy.

4. Results and discussion

Electron impact ionisation cross sections have been measured for the processes

$$e + Kr^{q+} \rightarrow Kr^{(q+1)+} + 2e \qquad (q = 1, 2, 3) \tag{3}$$

for energies below the threshold up to 700 eV. The resulting cross section data are listed in table 1 together with the total experimental error including the statistical uncertainty at 95% confidence level. The measured cross sections $\sigma_{q,q+1}$ $(q = 1, 2, 3)$ are displayed in figure 2. The error bars mark the total experimental uncertainties for each measured data point.

In the following the experimental results for the different ion charge states will be discussed separately.

4.1. Kr^{1+}

The atomic structure of Kr^{1+} ions is characterised by an Ar core with a $3d^{10}4s^24p^5$ outer-shell configuration. The ionisation potentials for these subshells are 107, 41 and 24.4 eV, respectively. Ionisation of the 3d subshell leads to an autoionising state so that double ionisation results. Hence, the only bound electrons contributing to direct single ionisation are from the 4s and 4p subshells. In principle, excitation of a 3d electron to a state (n, l) with subsequent autoionisation can also contribute to single ionisation. It is expected, however, that similar to the case of Xe^+ (Griffin *et al* 1984) the direct processes account for almost all of the observed ionisation. This expectation is supported by the close agreement of the measured cross section $\sigma_{1,2}$ with the

Table 1. Electron impact ionisation cross sections $\sigma_{q,q+1}$ ($q = 1, 2, 3$) for Kr^{q+} ions. Estimated total uncertainties are given including the statistical error at 95% confidence level.

(*a*) $\sigma_{1,2}$: $Kr^{1+} \rightarrow Kr^{2+}$.

Electron energy (eV)	Cross section (10^{-17} cm^2)	Electron energy (eV)	Cross section (10^{-17} cm^2)	Electron energy (eV)	Cross section (10^{-17} cm^2)
15.0	0.04 ± 0.07	50.0	17.2 ± 1.1	190.0	14.4 ± 0.9
18.0	−0.10 ± 0.29	51.9	17.5 ± 1.1	200.0	14.2 ± 0.9
21.0	0.05 ± 0.07	53.9	18.0 ± 1.1	210.0	13.9 ± 0.9
23.0	0.01 ± 0.05	56.0	18.1 ± 1.1	230.0	13.7 ± 0.9
24.0	0.48 ± 0.09	58.0	18.5 ± 1.2	240.0	13.5 ± 0.8
25.0	1.36 ± 0.16	60.0	18.6 ± 1.2	250.0	13.0 ± 0.8
26.0	2.19 ± 0.19	62.1	18.9 ± 1.2	270.0	12.8 ± 0.8
27.0	3.07 ± 0.23	66.0	19.6 ± 1.2	280.0	12.0 ± 0.7
28.0	3.65 ± 0.25	70.0	19.9 ± 1.2	290.0	11.9 ± 0.7
29.0	4.62 ± 0.32	75.0	19.8 ± 1.2	310.0	11.7 ± 0.7
30.0	6.45 ± 0.41	80.0	19.8 ± 1.2	330.0	11.2 ± 0.7
30.8	7.37 ± 0.46	85.0	19.3 ± 1.2	350.0	10.9 ± 0.7
32.0	8.73 ± 0.56	90.0	19.3 ± 1.2	371.0	10.5 ± 0.6
33.0	10.1 ± 0.6	95.0	18.9 ± 1.2	390.0	10.2 ± 0.6
34.0	10.7 ± 0.7	100.0	18.6 ± 1.2	410.0	9.65 ± 0.60
35.0	11.6 ± 0.7	105.0	18.4 ± 1.2	430.0	9.39 ± 0.58
36.0	12.4 ± 0.8	110.0	18.2 ± 1.1	450.0	9.30 ± 0.58
37.0	12.6 ± 0.8	120.0	17.4 ± 1.1	475.0	8.84 ± 0.55
38.5	13.4 ± 0.8	130.0	17.3 ± 1.1	500.0	9.06 ± 0.56
40.0	14.5 ± 0.9	140.0	16.5 ± 1.0	530.0	8.32 ± 0.52
42.0	15.0 ± 0.9	150.0	16.0 ± 1.0	565.0	7.75 ± 0.48
44.0	15.4 ± 1.0	160.0	15.8 ± 1.0	605.0	7.33 ± 0.45
46.0	16.1 ± 1.0	170.0	15.6 ± 1.0	650.0	7.19 ± 0.45
48.0	16.6 ± 1.0	180.0	15.0 ± 0.9	700.0	6.56 ± 0.41

(*b*) $\sigma_{2,3}$: $Kr^{2+} \rightarrow Kr^{3+}$.

Electron energy (eV)	Cross section (10^{-17} cm^2)	Electron energy (eV)	Cross section (10^{-17} cm^2)	Electron energy (eV)	Cross section (10^{-17} cm^2)
21.0	0.26 ± 0.36	50.0	8.00 ± 0.58	180.0	8.22 ± 0.52
25.0	0.23 ± 0.28	52.5	8.35 ± 0.59	191.0	8.22 ± 0.56
30.0	0.01 ± 0.02	55.6	8.95 ± 0.62	201.0	8.01 ± 0.54
32.4	0.10 ± 0.13	57.5	9.25 ± 0.65	210.0	7.77 ± 0.52
33.6	0.25 ± 0.09	60.3	9.85 ± 0.67	220.0	7.52 ± 0.48
34.8	0.96 ± 0.13	65.5	10.2 ± 0.7	240.0	7.13 ± 0.47
35.1	1.53 ± 0.16	70.5	10.5 ± 0.7	260.0	6.77 ± 0.43
35.5	1.61 ± 0.15	75.5	10.5 ± 0.7	280.0	6.56 ± 0.42
36.1	1.87 ± 0.15	80.0	10.3 ± 0.7	300.0	6.18 ± 0.40
36.5	2.33 ± 0.17	85.0	10.6 ± 0.7	321.0	6.04 ± 0.39
37.1	3.00 ± 0.21	90.2	10.5 ± 0.7	339.0	5.77 ± 0.37
37.7	3.16 ± 0.23	95.2	10.5 ± 0.7	360.0	5.67 ± 0.37
38.8	3.75 ± 0.25	99.6	10.3 ± 0.7	369.0	5.30 ± 0.33
39.8	4.15 ± 0.27	105.0	10.4 ± 0.7	380.0	5.03 ± 0.32
41.0	4.66 ± 0.30	110.0	10.3 ± 0.7	400.0	5.24 ± 0.34
42.1	5.04 ± 0.32	116.0	9.85 ± 0.62	420.0	4.97 ± 0.32
43.1	5.46 ± 0.34	120.0	9.63 ± 0.61	450.0	4.83 ± 0.31
44.3	5.87 ± 0.38	130.0	9.46 ± 0.59	476.0	4.33 ± 0.28
45.2	6.53 ± 0.53	135.0	9.15 ± 0.58	500.0	4.19 ± 0.27
45.5	6.48 ± 0.41	140.0	9.08 ± 0.57	530.0	3.98 ± 0.25
46.6	7.02 ± 0.44	151.0	8.97 ± 0.56	560.0	3.87 ± 0.25
47.8	7.31 ± 0.46	161.0	8.79 ± 0.55	600.0	3.65 ± 0.23
49.3	7.49 ± 0.47	170.0	8.45 ± 0.53	650.0	3.47 ± 0.22

Table 1. (continued)

(*c*) $\sigma_{3,4}$: $Kr^{3+} \rightarrow Kr^{4+}$.

Electron energy (eV)	Cross section (10^{-17} cm^2)	Electron energy (eV)	Cross section (10^{-17} cm^2)	Electron energy (eV)	Cross section (10^{-17} cm^2)
30.3	-0.06 ± 0.17	94.8	4.42 ± 0.29	240.0	2.94 ± 0.19
35.4	0.00 ± 0.19	100.0	4.40 ± 0.29	250.0	2.92 ± 0.18
40.4	0.08 ± 0.14	105.0	4.44 ± 0.28	270.0	2.81 ± 0.18
42.0	0.12 ± 0.16	110.0	4.47 ± 0.29	290.0	2.73 ± 0.17
45.4	0.09 ± 0.11	115.0	4.33 ± 0.27	300.0	2.65 ± 0.16
48.5	0.27 ± 0.09	120.0	4.24 ± 0.28	310.0	2.63 ± 0.17
50.0	0.97 ± 0.20	126.0	4.18 ± 0.26	330.0	2.53 ± 0.16
50.2	0.84 ± 0.14	132.0	4.09 ± 0.26	350.0	2.42 ± 0.15
52.2	1.27 ± 0.17	139.0	4.02 ± 0.25	370.0	2.29 ± 0.14
54.2	1.64 ± 0.21	145.0	4.04 ± 0.26	390.0	2.31 ± 0.14
56.5	2.33 ± 0.27	150.0	3.90 ± 0.25	400.0	2.18 ± 0.14
58.0	2.82 ± 0.27	160.0	3.84 ± 0.25	410.0	2.23 ± 0.14
59.7	3.03 ± 0.24	165.0	3.68 ± 0.24	430.0	2.10 ± 0.13
63.0	3.34 ± 0.25	170.0	3.71 ± 0.24	460.0	2.05 ± 0.13
66.2	3.61 ± 0.24	175.0	3.62 ± 0.23	490.0	1.96 ± 0.12
69.6	4.16 ± 0.28	180.0	3.69 ± 0.24	500.0	1.88 ± 0.12
72.9	3.98 ± 0.27	190.0	3.50 ± 0.22	520.0	1.90 ± 0.12
75.9	4.05 ± 0.28	200.0	3.43 ± 0.22	550.0	1.80 ± 0.11
79.1	4.24 ± 0.28	210.0	3.25 ± 0.21	580.0	1.74 ± 0.11
82.2	4.26 ± 0.28	220.0	3.21 ± 0.20	620.0	1.66 ± 0.10
85.8	4.34 ± 0.28	222.0	3.00 ± 0.19	650.0	1.57 ± 0.10
89.5	4.56 ± 0.30	230.0	2.96 ± 0.19	680.0	1.48 ± 0.09

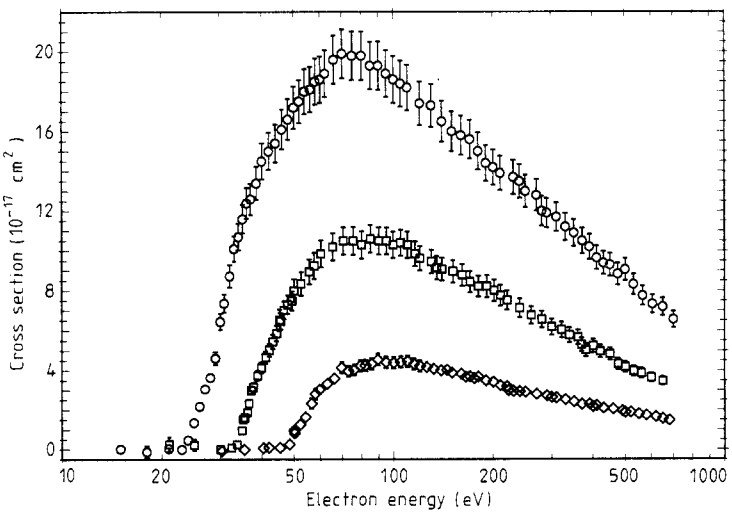

Figure 2. Present measurements of cross sections $\sigma_{q,q+1}$ for single ionisation of Kr^{q+} ions: ○, $\sigma_{1,2}$; □, $\sigma_{2,3}$; ◇, $\sigma_{3,4}$. Error bars show the total experimental uncertainties including the statistical error at 95% confidence level.

prediction (full curve in figure 3) of the semi-empirical Lotz formula (Lotz 1968)

$$\sigma_L = 4.5 \times 10^{-14}\ (\mathrm{cm^2\ eV^2}) \sum_i n_i \ln(E/P_i)/(EP_i) \tag{4}$$

where n_i is the number of electrons in the ith subshell, P_i is the ionisation potential of the ith subshell and E is the electron energy. The Lotz formula only describes direct ionisation of a single electron and does not include the excitation of an electron into autoionising states.

Also shown in figure 3 are the results of the semiclassical binary-encounter approximation (BEA) (Gryzinski 1965)

$$\sigma_{BEA} = \sigma_0 \sum_i g_i(x) n_i / P_i^2 \tag{5}$$

where $x = E/P_i$ and (for electron impact ionisation) $\sigma_0 = 6.56 \times 10^{-14}\ \mathrm{cm^2\ eV^2}$. The function $g_i(x)$ characterises the form of the cross section:

$$g_i(x) = \frac{1}{x}\left(\frac{x-1}{x+1}\right)^{3/2}\left[1+\frac{2}{3}\left(1-\frac{1}{2x}\right)\ln[2.7+(x-1)^{1/2}]\right]. \tag{6}$$

E, n_i and P_i are the same as for equation (4). As before, the summation extends over the 4p and 4s subshells and the BEA formula (equation (5)) gives an estimate only for the cross section of direct electron impact ionisation of a single electron. The differences of cross sections calculated from (4) and (5) are characteristic for the uncertainties of the general scaling rules for direct single ionisation.

While the threshold of $\sigma_{1,2}$ is expected at 24.4 eV, the experiment might indicate a slightly lower value, which is consistent with the presence of $^2P^o_{1/2}$ metastable ions

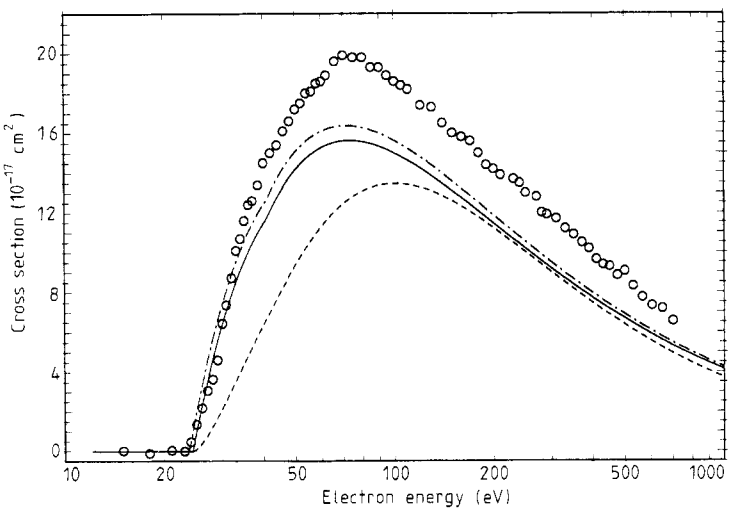

Figure 3. Comparison of the measured cross sections $\sigma_{1,2}$ (○) for single ionisation of Kr^{1+} ions with predictions of the Lotz formula (Lotz 1968) and the binary encounter approximation (BEA) (Gryzinski 1965) including contributions from 4p and 4s subshells: (——), Lotz formula for ground-state parent ion beam; (- - -), BEA for ground-state parent ion beam; (— · —), Lotz formula for an assumed 100% population of the $^2P^o_{1/2}$ metastable state in the parent ion beam.

(0.67 eV excitation energy) in the parent ion beam. The low excitation energy, however, can change the cross section only slightly as the Lotz calculation for an assumed 100% metastable parent ion beam shows (chain curve in figure 3).

4.2. Kr^{2+}

Figure 4 shows our measured cross sections $\sigma_{2,3}$ for single ionisation of Kr^{2+} ions together with the experimental results of Danjo *et al* (1984) and Gregory (1985). Also shown are the results of Lotz and BEA calculations from (4) and (5) for direct single ionisation of the 4p and 4s subshells with ionisation potentials 36.95 and 52 eV, respectively. All three sets of experimental data give different maximum cross sections. Also, the cross section function of Danjo *et al* shows a pronounced structure at an electron energy of about 150 eV which can hardly be seen in the two other measurements. Nevertheless, error bars of ±15% around the data of Danjo *et al* would include all experiments. None of these, however, quotes a total uncertainty exceeding ±9% at maximum, which indicates a systematic problem.

In order to exclude an error in our data-taking procedure and in the data processing, we rechecked the correct measurement of electron and ion currents, the complete transmission of parent and product ions, the detector efficiency, the electronics and computer programs used; we measured at different ion currents and ion energies and we found no inconsistencies. So we are sure that no systematic experimental error can account for the observed discrepancies.

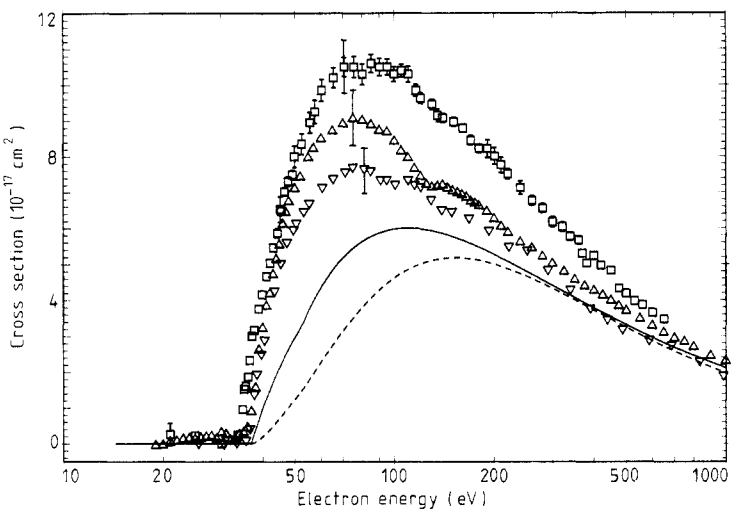

Figure 4. Cross sections $\sigma_{2,3}$ for the single ionisation of Kr^{2+} ions: □, present measurements (error bars show the statistical uncertainty at 95% confidence level); △, measurements of Danjo *et al* (1984) (statistical error is typically 1%); ▽, measurements of Gregory (1985) (statistical errors do not exceed symbol size). The outer error bars at about 75 eV mark the total experimental uncertainties including the statistical errors at good confidence level for each data set. The curves represent predictions of the Lotz formula (——) and the BEA (- - -) for the ionisation of Kr^{2+} ground-state ions including contributions from 4p and 4s subshells.

As suggested already for Kr^{1+} ions, there may be different amounts of metastable ions in the parent ion beam. Indeed, a closer look at the threshold region shows the possible influence of low-lying $4p^4$ metastable states ($^3P_1$, $^3P_0$, $^1D_2$, $^1S_0$) with excitation energies not higher than 4.10 eV and a group of $4p^34d$ metastable states ($^5D_4^o$, $^3F_4^o$, $^3G_4^o$, $^3G_5^o$, $^1G_4^o$, $^3F_4^o$) with excitation energies up to 21.70 eV.

The threshold in our data from figure 4 indicates a strong population of the *low*-energy metastable group while the data of Danjo *et al* appear to be slightly influenced by the *high*-energy metastable group. By tuning our ion source we succeeded in changing the composition of our Kr^{2+} ion beam and obtained a considerable fraction of ions in the high-lying metastable states. Figure 5 shows a comparison of measured cross sections $\sigma_{2,3}^{I}$ and $\sigma_{2,3}^{II}$ for the two different Kr^{2+} ion beam compositions. The lower cross sections $\sigma_{2,3}^{I}$ are our data from figure 4 and $\sigma_{2,3}^{II}$ is the result with increased metastable content in the beam. The threshold of the new data set $\sigma_{2,3}^{II}$ is compatible with the presence of $^3F_4^o$ metastable ions with an ionisation energy of 15.2 eV. Below this threshold the measured cross section is zero.

When we assume that the change in cross section size from one beam composition to the other is only due to a change in the direct ionisation probability, then the Lotz formula should give a reasonable picture for the size of the possible difference $\sigma_{2,3}^{II} - \sigma_{2,3}^{I}$ of cross sections measured with and without the high-energy metastable contribution. The full curve in figure 5 is a Lotz calculation under the assumption that all ions are in the $^1S_0$ metastable state of Kr^{2+}; i.e. $P_1 = 32.85$ eV for 4p subshell and $P_2 = 52$ eV for the 4s subshell. This curve represents the contribution of direct ionisation to $\sigma_{2,3}^{I}$. The two other curves in figure 5 represent Lotz calculations for direct ionisation

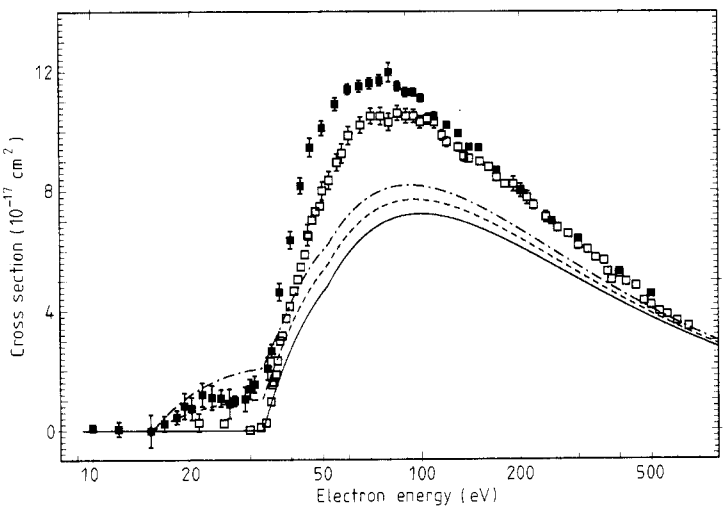

Figure 5. Comparison of measured cross sections $\sigma_{2,3}$ for Kr^{2+} ions obtained with different parent ion beam compositions (error bars show the statistical error at 95% confidence level): □, $\sigma_{2,3}^{I}$, ion beam contained no significant fraction of ions in high-lying metastable states; ■, $\sigma_{2,3}^{II}$, ion beam contained a considerable fraction of ions in high-lying metastable states. The curves represent results of the Lotz formula including contributions from the 4p and 4s subshells assuming different fractions of parent ions in low-lying ($^1S_0$) and high-lying ($^3F_4^o$) metastable states: (——), 100% population of the low-lying metastable state; (- - -), population of 15% high-lying and 85% low-lying metastable states; (— · —), population of 30% high-lying and 70% low-lying metastable states.

contributing to $\sigma^{II}_{2,3}$ assuming 15% (broken curve) and 30% (chain curve), respectively, of ions in the $^3F^o_4$ state ($P_1 = 15.2$ eV) while the rest is in the $^1S_0$ state. A comparison of the Lotz calculations shows that the differences between $\sigma^{I}_{2,3}$ and $\sigma^{II}_{2,3}$ can be explained well already by the difference in direct ionisation of Kr^{2+} ions in different metastable states.

A similar analysis for the data of Danjo *et al* results in a possible high-lying metastable ion content of about 4%. A correction of their measured cross section $\sigma_{2,3}$ to zero contribution from the high-energy metastable group leads to a slight reduction (about 3% at maximum), i.e. shift towards the data of Gregory.

So far we have obtained an idea of the possible influence of the high-energy metastable states of Kr^{2+} on the cross section $\sigma_{2,3}$. In figure 6 the influence of the low-energy metastable group is investigated. For comparison only the data of Gregory are shown together with our measurements $\sigma^{I}_{2,3}$. The full curve represents the Lotz formula for ground-state Kr^{2+} ions, and the broken curve is the same for 100% metastable $^1S_0$ Kr^{2+} ions. There is an indication in the data of Gregory for the presence of low-lying $^3P_1$, $^3P_0$ and even $^1D_2$ metastable ions in the beam. However, the excitation energy of these states is so low that their influence on the size of the cross section can be neglected. Hence, the difference of the Lotz cross sections for $^1S_0$ metastable and $^3P_2$ ground-state ions should account for most of the difference between our measured cross sections $\sigma^{I}_{2,3}$ and the data of Gregory. For comparison the dotted curve in figure 6 represents $\sigma^{I}_{2,3} - [\sigma_L(^1S_0) - \sigma_L(^3P_2)]$. Although the dotted curve is still above the data of Gregory, the total error bars do now overlap. In addition, a possible difference between EA contributions from the $^1S_0$ metastable and $^3P_2$ ground-state ions should be subtracted from the dotted curve, probably leading to still closer agreement with Gregory's data.

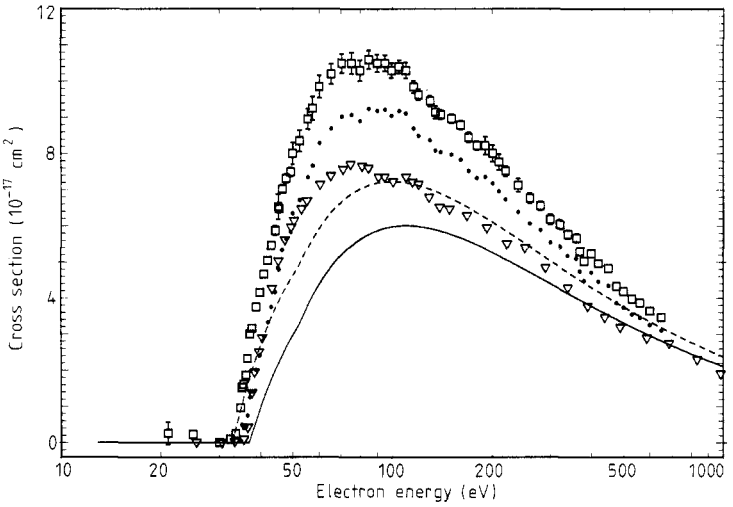

Figure 6. Comparison of the present experimental results $\sigma^{I}_{2,3}$ (□) for the single ionisation of Kr^{2+} ions with no significant fraction of ions in high-lying metastable states with the measurements of Gregory (▽). (Error bars show the statistical error, see figure 4.) Also shown are the prediction of the Lotz formula for ground-state Kr^{2+} ions (——) and the result of the Lotz formula for 100% population of the $^1S_0$ metastable state (- - -). The dotted curve results by subtracting the difference between broken curve and full curve from the measured cross section $\sigma^{I}_{2,3}$.

From our discussion we conclude that our experimental cross sections $\sigma^{I}_{2,3}$ are for Kr^{2+} ions in (low-lying) metastable states while the data of Gregory closely resemble the cross sections for ground-state Kr^{2+} ions.

4.3. Kr^{3+}

Figure 7 shows our measured cross sections $\sigma_{3,4}$ for single ionisation of Kr^{3+} ions together with the experimental results of Gregory *et al* (1983). Also shown are the Lotz (full curve) and BEA (broken curve) calculations for $4p^3\ {}^4S^o_{3/2}$ ground-state ions with contributions from the 4p and 4s subshells. The calculated ionisation potentials are 50 eV for the 4p and 67 eV for the 4s subshell (Gregory *et al* 1983) with an estimated uncertainty of ±1 eV. The extrapolated spectroscopic value for the ionisation potential of the 4p shell is 52.5 eV (Moore 1970).

The experimental threshold of our data is about 45.0 eV, that of the Oak Ridge measurements roughly 2 eV higher. Both data sets indicate the presence of metastable ions in the parent beam. Again, we used the Lotz formula (equation (4)) to visualise cross section differences for metastable and ground-state ions. The (— — —) curve in figure 7 is calculated for metastable ions with an assumed 3 eV excitation energy to fit the Oak Ridge data; the chain curve is for an assumed 5 eV excitation energy which would explain the onset of our experimental data. We do not have any more detailed information about which metastable states may be involved in these measurements.

As in the case of Kr^{2+}, a dotted curve is calculated representing an approximation for the ground-state cross section: $\sigma_{2,3} - [\sigma_L(\text{metastable state}) - \sigma_L(\text{ground state})]$. The

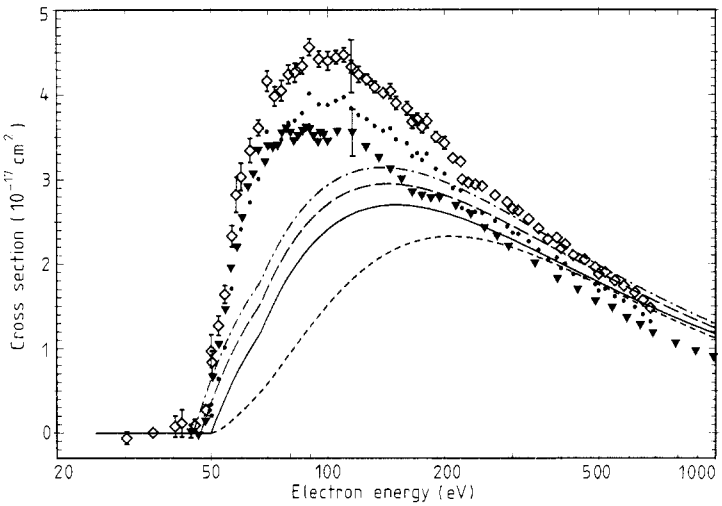

Figure 7. Cross sections $\sigma_{3,4}$ for the single ionisation of Kr^{3+} ions: ◇, present measurements; ▼, measurements of the Oak Ridge group (Gregory *et al* 1983). (Inner error bars mark the statistical error at good confidence level; outer error bars show total experimental uncertainties.) The predictions of the Lotz formula (——) and the BEA (- - -) for the ionisation of Kr^{3+} ground-state ions (threshold energy of 50 eV) including contributions from 4p and 4s subshells are shown as well as Lotz calculations with threshold energies of 47 eV (— — —) and 45 eV (— · —). The dotted curve results by subtracting the difference between chain curve and full curve from the present measurements of $\sigma_{3,4}$.

dotted curve is close to the measurement of Gregory *et al*, which might indicate a low fraction of metastable ions in their parent ion beam.

The agreement of Lotz cross sections with the experimental data at electron energies above roughly 200 eV indicates at most small contributions of indirect processes in this region. Indeed, McGuire (1983) calculated EA from the 3s, 3p, 3d and 4s subshells of ground-state Kr^{3+} ions using the plane-wave Born approximation and found not more than 20% contribution of the indirect processes to total (single) ionisation at high electron energies above 500 eV. These calculations also show that ionisation of the 3d subshell does not contribute to single ionisation. At energies around 100 eV, however, none of the calculations can reproduce the measured cross sections. There seems to be a contribution similar in shape to the one observed in single ionisation of Xe^{3+} ions (Achenbach *et al* 1984, Gregory *et al* 1983) or with double ionisation of I^+ and Xe^+ ions (Müller *et al* 1984). This same feature might also be present in the measurements with Kr^{2+} ions. Work is in progress to understand such structures better in ionisation cross sections (Younger 1986).

5. Conclusions

The present measurements clearly demonstrate the complications introduced to the interpretation of ionisation cross section data by the presence of metastable ions in the parent ion beams. Three experiments discussed here using different ion sources (electron-beam ion source, this work; electron-cyclotron-resonance-type ion source, Danjo *et al*; Penning ion gauge, Gregory *et al*) give significantly different cross sections. It would certainly be desirable for ionisation experiments to identify the metastable states and their fractions in the ion beam. This demand, however, could only be satisfied so far in few cases (see e.g. Falk *et al* 1983b) and it will become more difficult to attack this problem as high charge states of complex ions produced in hot-plasma ion sources will be investigated. Nevertheless, the data obtained in experiments like the present one are useful since the plasma environments for which cross section data are needed produce these same ions in a mixture of metastable states.

The experimental data for the isonuclear series of Kr^{q+} ions with $q = 1$, 2 and 3 show an increasing relative contribution to single ionisation that cannot easily be explained by direct or indirect ionisation mechanisms. While $\sigma_{1,2}$ is reproduced fairly well by the Lotz formula, the cross sections $\sigma_{2,3}$ and $\sigma_{3,4}$ only approach the Lotz formula at high electron energies. At energies between about 50 and 150 eV the measurements significantly exceed the expected values for direct single ionisation. If the enhancement were due to common EA involving, for example, the 3d subshell, then it should extend also to high energies as, for example, the calculations of McGuire (1983) show. Griffin *et al* (1984) have tried to explain a similar feature between 50 and 150 eV in Xe^{3+} single ionisation data on the basis of term dependence of excitation processes. In their calculations, however, only the high-energy part of the additional contributions could be explained reasonably well while at lower energy (50 to 80 eV) ionisation strength observed experimentally was missing in the calculations. The differences may indicate that a new method of theoretical treatment is required for ionisation processes of complex ions. Younger (1986) has shown recently for ionisation of Cs^+ that giant atomic resonances can produce cross section shapes as discussed above and it can be expected that this new concept applies to a wide variety of complex atomic systems.

Acknowledgments

The authors acknowledge the help of R Sauer during the present measurements. We are grateful to Professor B Fricke, University of Kassel, and Professors Wunner and Ruder, University of Tübingen, for communicating calculated binding energies of electrons in different subshells of krypton ions. The work reported here was supported by Deutsche Forschungsgemeinschaft.

References

Achenbach C, Müller A, Salzborn E and Becker R 1984 *J. Phys. B: At. Mol. Phys.* **17** 1405-25
Crandall D H, Phaneuf R A, Falk R A, Belić D S and Dunn G H 1982 *Phys. Rev.* A **25** 143-53
Crandall D H, Phaneuf R A, Hasselquist B E and Gregory D C 1979 *J. Phys. B: At. Mol. Phys.* **12** L249-56
Danjo A, Matsumoto A, Ohtani S, Suzuki H, Tawara H, Wakiya K and Yoshino M 1984 *J. Phys. Soc. Japan* **53** 4091-3
Falk R A, Dunn G H, Gregory D C and Crandall D H 1983a *Phys. Rev.* A **27** 762-70
Falk R A, Dunn G H, Griffin D C, Bottcher C, Gregory D C, Crandall D H and Pindzola M S 1981 *Phys. Rev. Lett.* **47** 494-7
Falk R A, Stefani G, Camilloni R, Dunn G H, Phaneuf R A, Gregory D C and Crandall D H 1983b *Phys. Rev.* A **28** 91-8
Gregory D C 1985 *Nucl. Instrum. Methods Phys. Res.* B **10/11** 87-91
Gregory D C and Crandall D H 1983 *Phys. Rev.* A **27** 2338-41
Gregory D C, Dittner P F and Crandall D H 1983 *Phys. Rev.* A **27** 724-36
Griffin D C, Bottcher C, Pindzola M S, Younger S M, Gregory D C and Crandall D H 1984 *Phys. Rev.* A **29** 1729-41
Gryzinski M 1965 *Phys. Rev.* **138A** 336-58
Howald A M, Gregory D C, Meyer F W, Phaneuf R A, Müller A, Djurić N and Dunn G H 1986 *Phys. Rev.* A **33** 3779-86
LaGattuta K J and Hahn Y 1981 *Phys. Rev.* A **24** 2273-6
Lotz W 1968 *Z. Phys.* **216** 241-7
McGuire E J 1983 *Phys. Rev.* A **28** 2091-5
Moore C E 1970 *Atomic Energy Levels* NSRDS-NBS 34 (Washington, DC: US Govt Printing Office)
Mueller D W, Morgan T J, Dunn G H, Gregory D C and Crandall D H 1985 *Phys. Rev.* A **31** 2905-13
Müller A, Achenbach C, Salzborn E and Becker R 1984 *J. Phys. B: At. Mol. Phys.* **17** 1427-44
Müller A, Hofmann G, Tinschert K, Sauer R, Salzborn E and Becker R 1987 *Nucl. Instrum. Methods Phys. Res.* in press
Müller A, Huber K, Tinschert K, Becker R and Salzborn E 1985a *J. Phys. B: At. Mol. Phys.* **18** 2993-3009
Müller A and Salzborn E 1979 *Nucl. Instrum. Meth.* **164** 607-8
Müller A, Salzborn E, Frodl R, Becker R, Klein H and Winter H 1980 *J. Phys. B: At. Mol. Phys.* **13** 1877-99
Müller A, Tinschert K, Aschenbach C, Salzborn E and Becker R 1985b *Nucl. Instrum. Methods Phys. Res.* B **10/11** 204-6
Peart B and Dolder K 1975 *J. Phys. B: At. Mol. Phys.* **8** 56-62
Rinn K, Müller A, Eichenauer H and Salzborn E 1982 *Rev. Sci. Instrum.* **53** 829-37
Tawara H, Kato T and Ohnishi M 1985 *Japan. Inst. Plasma Phys. Rep.* IPPJ-AM-37
Woodruff P R, Hublet M-C and Harrison M F A 1978 *J. Phys. B: At. Mol. Phys.* **11** L305-8
Younger S 1986 private communication